Hindawi
International Journal of Aerospace Engineering
Volume 2021, Article ID 6683684, 11 pages
https://doi.org/10.1155/2021/6683684

Research Article

Onboard Trajectory Generation of Hypersonic Morphing Aircraft

Chenxin Zhang,[1] **Yankun Zhang**,[2] **and Changzhu Wei**[2]

[1]*National University of Defense Technology, Hunan 410073, China*
[2]*Harbin Institute of Technology, Harbin 150001, China*

Correspondence should be addressed to Changzhu Wei; weichangzhu@hit.edu.cn

Received 16 November 2020; Revised 26 January 2021; Accepted 26 February 2021; Published 15 March 2021

Academic Editor: Rosario Pecora

Copyright © 2021 Chenxin Zhang et al. This is an open access article distributed under the Creative Commons Attribution License, which permits unrestricted use, distribution, and reproduction in any medium, provided the original work is properly cited.

In this paper, a trajectory optimization strategy for the hypersonic morphing aircraft is proposed, and the AMPI method is used to generate the online trajectory with initial state errors. Firstly, the aerodynamic model and propulsion model of the hypersonic morphing aircraft were established considering the wingspan and the scramjet. Secondly, the optimization strategy was proposed via Gauss pseudospectral method considering the control variables including angle of attack (AOA) and wingspan. The optimized trajectory met the final constraints and path constraints with the objective to minimize the time of the ascent phase. Then, the AMPI method was used to generate online trajectory without solving OCP or NLP on the base of trajectory database calculated by the optimization strategy. The simulation results indicate high accuracy of AMPI method and the final errors corresponding to different initial errors were acceptable. The mean value of the CPU time of the method was about 0.1 second, which shows real-time capability.

1. Introduction

Inspired by birds and insects that can change their shapes in no time during the flight to adapt to the environment, aircraft designers proposed the idea of morphing aircraft [1]. A morphing aircraft can adaptively change its shape to achieve the optimal performance in different tasks and environments, which brings tantalizing prospect to overcome the obstacles that are hard to solve currently.

Morphing aircrafts have been developing rapidly since Rockwell proposed the concept of active flexible wing (AFW) in 1985 [2]. NASA finished AFW project and "Active Aeroelastic Wing" (AAW) project in 2000 [3]. The United States Air Force (USAF) in cooperation with DARPA launched the "Smart Wing" project based on NASA's technology storage [4]. Moreover, they proposed an idea of bending the wings' chord with shape memory alloys and performed a wind tunnel experiment with a 30% scaled X-47 UAV model to verify such idea [5]. DARPA carried out "Morphing Aircraft's Structure" (MAS) project to realize the idea of bending the wing shape with a new structure and a new material to adapt to the environmental change [6]. In addition, New Generation and Lockheed Martin carried out low-speed flying experiments and high-speed wind tunnel experiments of morphing aircraft. Based on the rapid development of morphing aircraft, NASA forecasted that morphing aircrafts would be widely used in the field of aviation by 2030 [7].

With the rapid development of morphing aircrafts, many researches on trajectory optimization for morphing vehicle have been done. Jasa [8] proposed a trajectory optimization approach based on surrogate model. Maxwell [9] presented an optimization strategy to minimize peak heat flux and deceleration of entry vehicle. Wu [10] presented an optimal flight planning method for Z-shaped morphing UAV. Peng [11] optimized the glide phase of hypersonic morphing aircraft through multiobjective optimization method. However, these methods are not acceptable for onboard generation of hypersonic morphing aircraft because these algorithms are time-consuming.

In addition, for common trajectory optimization, Gauss pseudospectral method is a popular method to solve optimal control problems and has been widely used in trajectory optimization [12–14]. But GPM also needs to solve the NLP by direct method. Significant progress of convex optimization has also been achieved in recent years [15–19]. Many

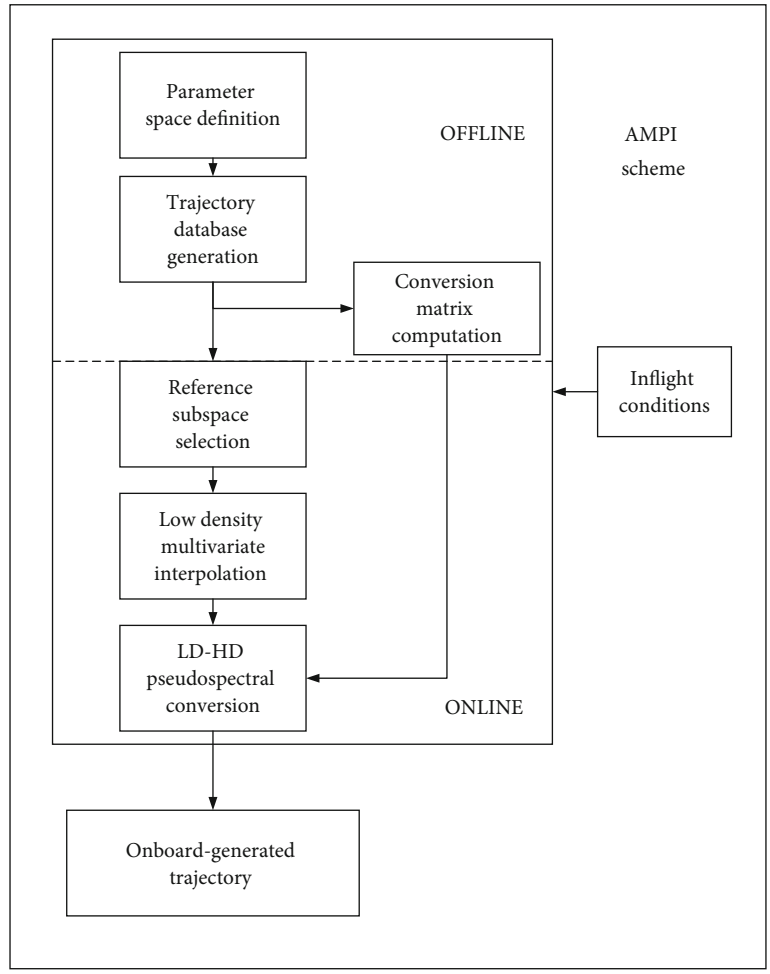

Figure 1: Scheme of AMPI.

convexification techniques were used to convert the NLP formulation of the trajectory optimization problem into a convex form. In this way, the strategy avoids the complicated process to solve NLP, and the global convergence of the strategy was improved. On the basis of convexification technique, Chai [20, 21] proposed an effective strategy to deal with both deterministic constraints and probabilistic constraints via convex optimization. They transcribed the chance constraints into deterministic constraints, and the simulations showed the effectiveness and achieved enhanced computational performance.

However, because of the coupling of wingspan and aerodynamic coefficient, the optimal morphing strategy of morphing aircraft during the flight becomes complicated, and the generation of the optimal trajectory takes a long time, which cannot meet the requirements of online computing, especially for hypersonic vehicle.

Many parameters have a great influence on the aircraft's performance, such as wingspan and sweepback. In this paper, we focus on the wingspan. An aircraft can significantly change its performance by changing the wingspan. For example, by increasing the wingspan, an aircraft can increase the aircraft's lift and drag, thus varying the aircraft's lift-drag ratio and producing great influence on the performance of the aircraft. In this way, in the ascent phase, a wide wingspan may enable the aircraft to fly higher but lead to a decrease of final speed. Conversely, reducing the wingspan will decrease the height but increase the aircraft's final speed.

Table 1: The value of the initial states and target final states.

Number	Initial states	Target final states
Height	17500m	26000m
Velocity	1000m/s	1795m/s
Path angle	3.5 deg	0 deg
Mass	3000kg	/
AOA	1 deg	/
Wingspan	0.6	/

In this paper, we proposed a trajectory optimization strategy for the morphing aircraft considering the control variables including AOA and wingspan. After obtaining the optimal offline trajectory, the online trajectory was generated via AMPI [22] method, which shows real-time capability.

Because there is no need for the AMPI method to solve OCP or NLP, it shows high efficiency during generating

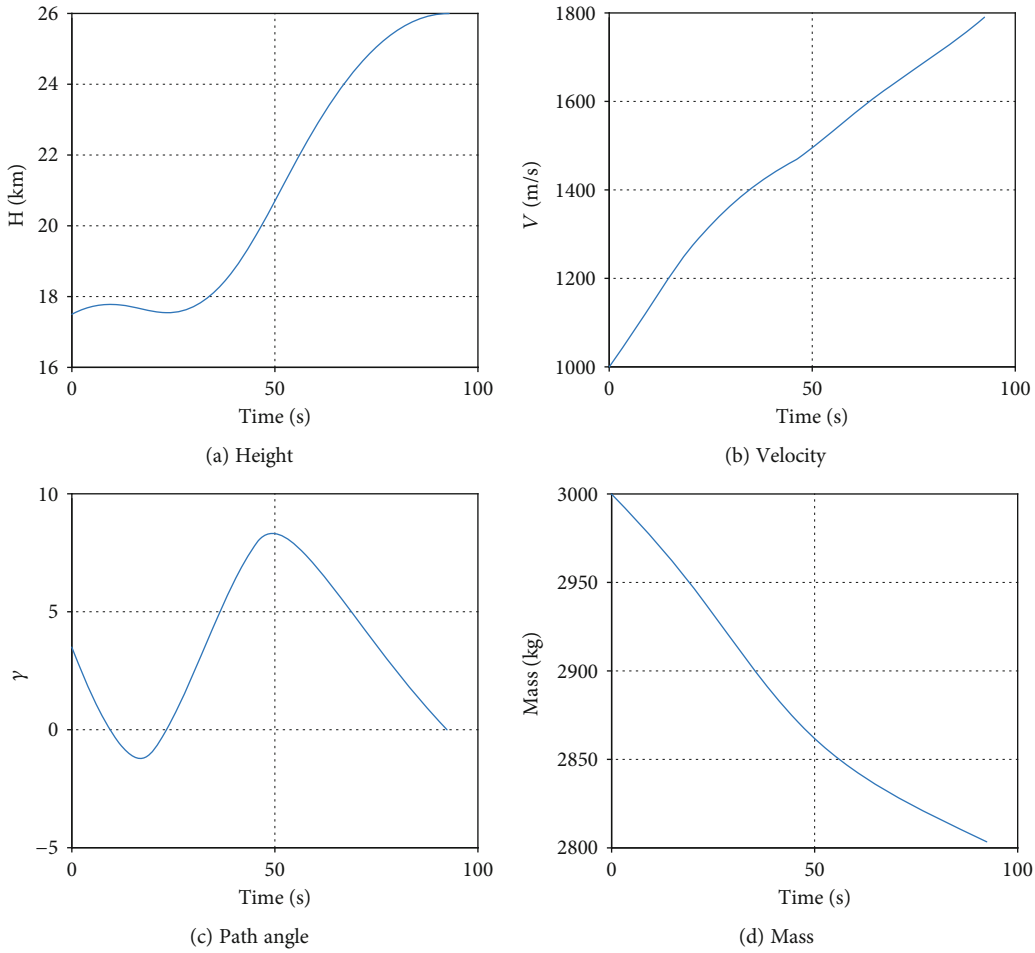

(a) Height (b) Velocity

(c) Path angle (d) Mass

Figure 2: The optimization trajectory.

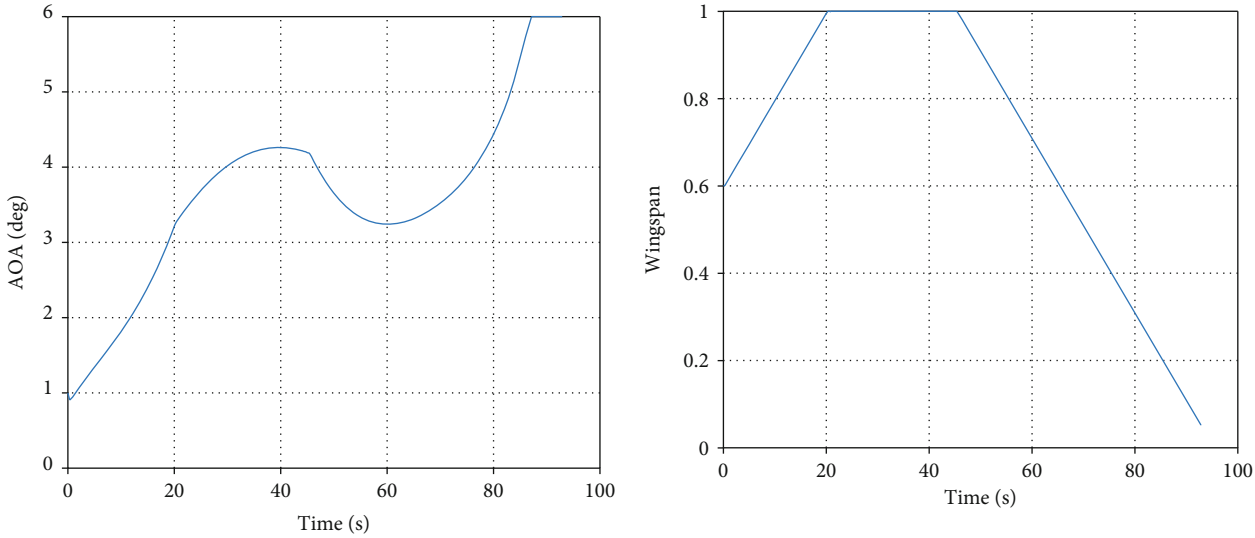

(a) AOA (b) Wingspan

Figure 3: The time history of control.

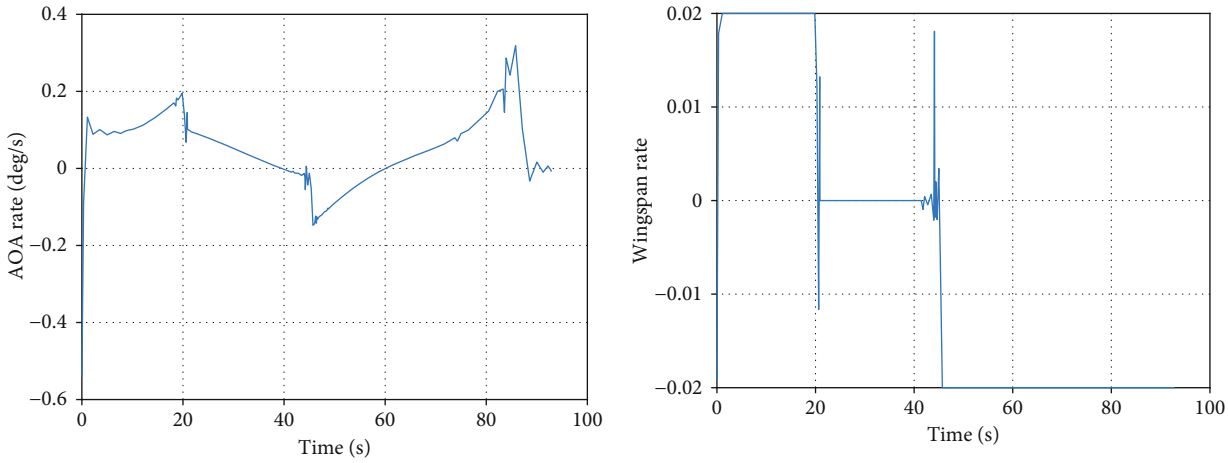

(a) AOA rate (b) Wingspan rate

Figure 4: The time history of the attack angle rate and wingspan rate.

trajectory. The calculation of AMPI just includes polynomial calculation and matrix multiplication. And both the AOA and wingspan vary continuously, which are suitable for polynomial fitting. Subsequently, AMPI is suitable for onboard trajectory generation of morphing aircraft.

2. Model

2.1. Dynamics. The motion of the ascent phase is described as follows:

$$\begin{cases} \dot{h} = v \sin\gamma \\ \dot{s} = v \cos\gamma \\ \dot{v} = \dfrac{T(\mathrm{Ma}, h, \alpha, \lambda)\cos\alpha - D}{m} - g\sin\gamma \\ \dot{\gamma} = \dfrac{L(\mathrm{Ma}, h, \alpha, \lambda) + T(\mathrm{Ma}, h, \alpha)\sin\alpha}{mv} - \left(\dfrac{g}{v} - \dfrac{v}{r}\right)\cos\gamma \\ \dot{m} = \dot{m}(\mathrm{Ma}, \alpha) \end{cases}, \tag{1}$$

where h is the height; s is the range; v is the velocity; γ is the path angle; L and D are the drag and lift, respectively; g is the gravity acceleration; α is angle of attack; λ is the wingspan; and m is the mass of the vehicle.

2.2. Aerodynamic Model. The drag and lift can be calculated as follows:

$$\begin{aligned} L &= C_L q S_{ref} \\ D &= C_D q S_{ref}, \end{aligned} \tag{2}$$

where C_L and C_D are the lift coefficient and drag coefficient, which are effect by both angle of attack and wingspan, respectively; q is the dynamic pressure defined as $q = 0.5\rho v^2$; and S_{ref} is reference area. C_L and C_D can be calculated as follows:

$$\begin{aligned} C_L &= 0.5C_{L0}\left(1 + \lambda^{A_1}\sqrt{A_2 Ma}\right)/2 + A_3\alpha/Ma \\ C_D &= 0.5C_{D0}\left(1 + \lambda^{B_1}\sqrt{B_2 Ma}\right)/2 + B_3\alpha^2/Ma + B_4\alpha/Ma, \end{aligned} \tag{3}$$

where A_1, A_2, A_3 and B_1, B_2, B_3, B_4 are the coefficients determined by the vehicle and C_{L0} and C_{D0} can be calculated as follows:

$$\begin{aligned} C_{L0} &= a_1\alpha + a_2 \\ C_{D0} &= b_1\alpha^2 + b_2\alpha + b_3, \end{aligned} \tag{4}$$

where a_1, a_2 and b_1, b_2, b_3 are the coefficients determined by the vehicle.

2.3. Propulsion Model. The thrust can be calculated as follows:

$$T = C_T q S_{ref}, \tag{5}$$

where C_T is the thrust coefficient.

Since the engine is basically an air breather, C_T is affected by both the velocity and angle of attack:

$$C_T = C_1 + C_2\alpha + C_3\alpha/Ma + C_4/Ma, \tag{6}$$

where C_1, C_2, C_3, C_4 are the coefficients determined by the propulsion system.

The mass rate can be calculated as follows:

$$\dot{m} = k\rho v S_{\mathrm{cap}}, \tag{7}$$

where k is a coefficient defined by the propulsion system and S_{cap} is the capture area.

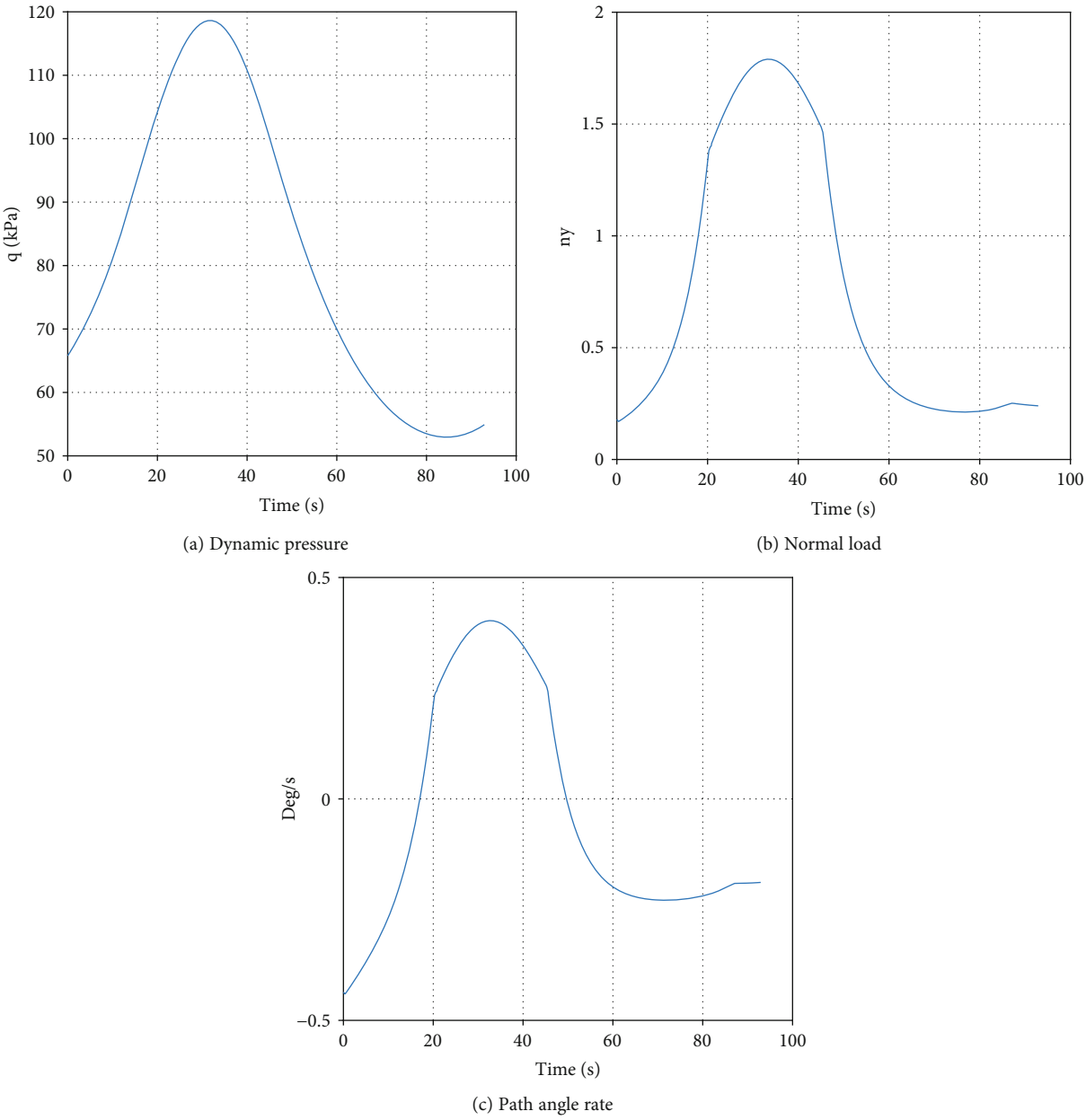

(a) Dynamic pressure

(b) Normal load

(c) Path angle rate

Figure 5: The time history of path constraints.

3. Optimal Trajectory Generation

In this section, we formulated the optimal control problem (OCP) of the ascent phase so that we can obtain the optimal trajectory. The OCP consists of state function, control variables, cost function, and constraints. The state function was augmented to limit the AOA rate and wingspan rate, thus minimizing the ascent time. We considered many constraints, such as dynamic pressure path angle rate, final states, and constraints of control variables. In this way, we can solve the ascent trajectory problem via Gauss pseudospectral method.

3.1. State Function. In the optimal control problem of the ascent phase, we changed the dynamic function into the following form by introducing angle of attack and wingspan:

$$\dot{\boldsymbol{x}} = \left[\dot{h}\dot{s}\dot{v}\dot{\gamma}\dot{m}\dot{\alpha}\dot{\lambda}\right]^T, \tag{8}$$

$$\boldsymbol{u} = \left[\dot{\alpha} \quad \dot{\lambda}\right]^T, \tag{9}$$

Since we introduced the angle of attack and wingspan into the state function, the dimension of the state of the optimal control problem was augmented from 5 to 7, so that the AOA rate and wingspan rate can be limited. It is worth noting that the wingspan rate was limited by the actuator, which prevents the wingspan from changing too fast especially during the hypersonic phase.

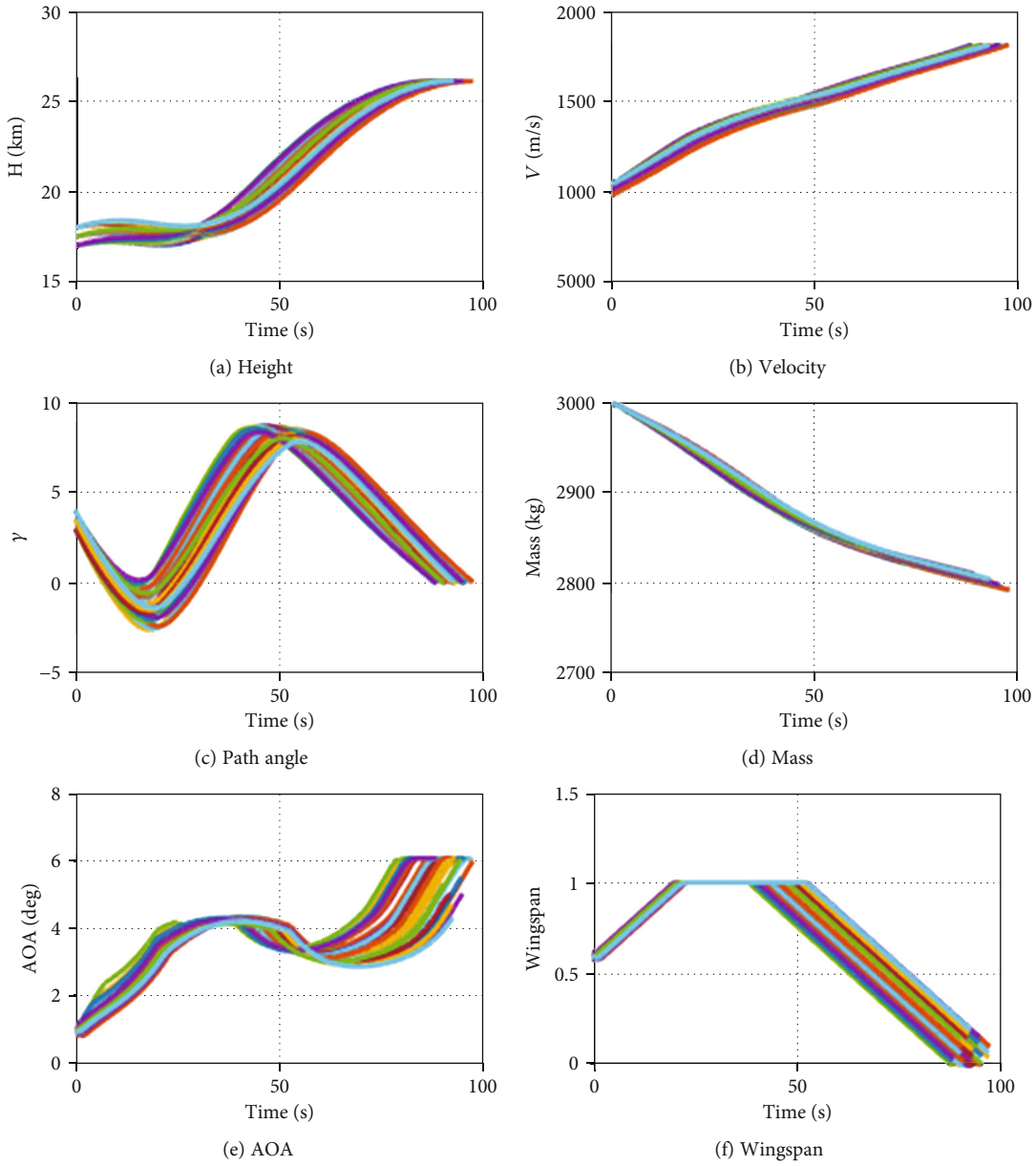

Figure 6: The offline database.

3.2. Cost Function. The objective is to minimize the time of the ascent phase:

$$J = t_f, \tag{10}$$

where t_f is the final time of the ascent phase.

3.3. Constraints. The constraints of control variables are as follows:

$$\begin{aligned} |\dot{\alpha}| &< \dot{\alpha}_{\max} \\ |\dot{\lambda}| &< \dot{\lambda}_{\max}, \end{aligned} \tag{11}$$

where $\dot{\alpha}_{\max}$ is the maximum AOA rate and $\dot{\lambda}_{\max}$ is the maximum wingspan rate.

The path constraints are as follows:

$$\begin{aligned} \alpha_{\min} < \alpha < \alpha_{\max} \\ \lambda_{\min} < \lambda < \lambda_{\max} \\ q_{\min} < q < q_{\max} \\ n_y < n_{y\,\max} \\ |\dot{\gamma}| < \dot{\gamma}_{\max}, \end{aligned} \tag{12}$$

where $\alpha_{\max}, \lambda_{\max}, q_{\max}$ are the maximum AOA, maximum wingspan, and maximum dynamic pressure, respectively; $\alpha_{\min}, \lambda_{\min}, q_{\min}$ are the minimum AOA, minimum wingspan, and minimum dynamic pressure, respectively; n_y is the vertical load factor; $n_{y\,\max}$ is the maximum vertical load factor;

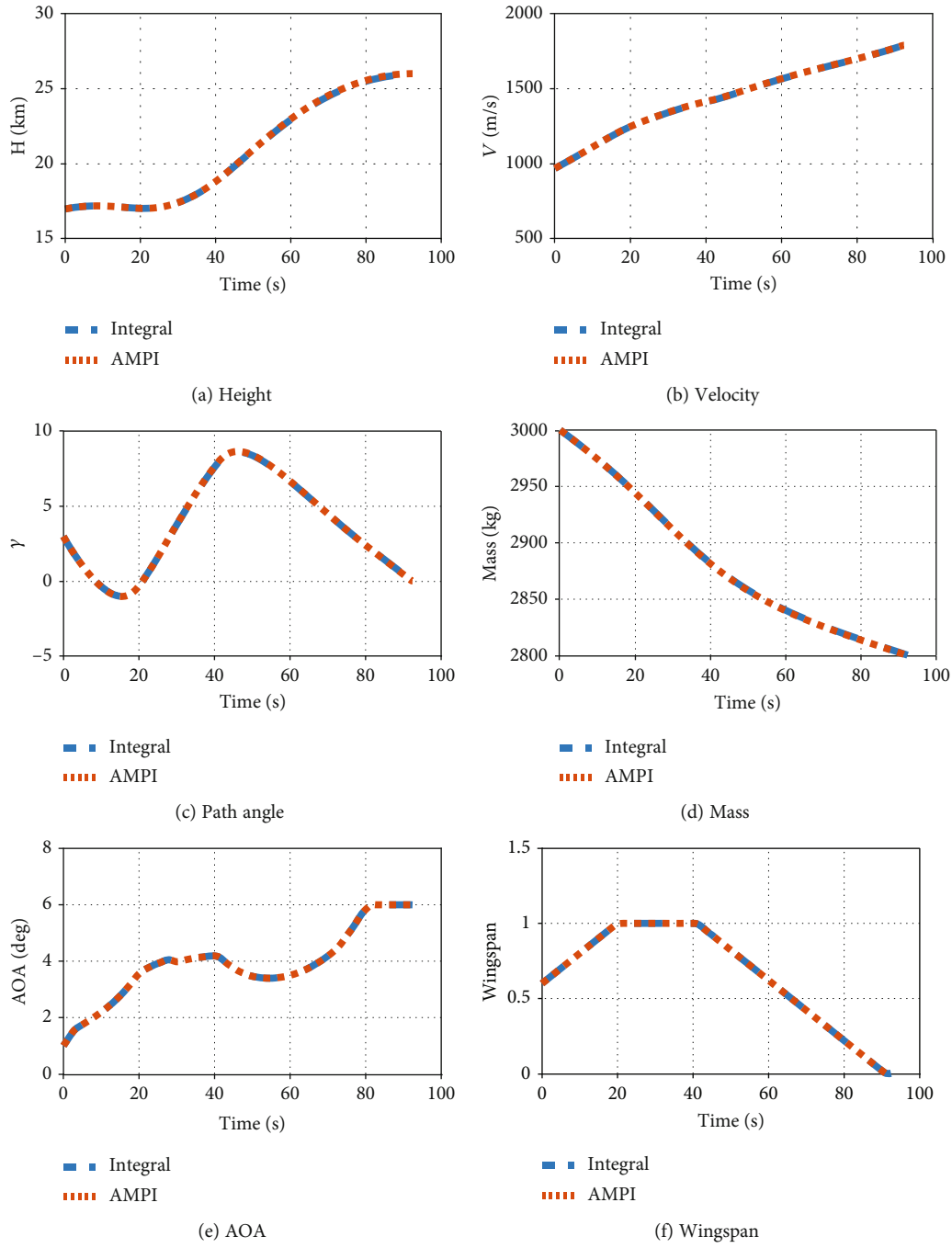

Figure 7: AMPI vs. integral.

and $\dot{\gamma}_{\max}$ is the maximum path angle rate. The angle of attack and dynamic pressure are limited by the propulsion system. The wingspan is constrained by the minimum and maximum wingspan.

The terminal constraints are as follows:

$$\begin{aligned} h_{\mathrm{f\ min}} < h_{\mathrm{f}} < h_{\mathrm{f\ max}} \\ v_{\mathrm{f\ min}} < v_{\mathrm{f}} < v_{\mathrm{f\ max}} \\ \gamma_{\mathrm{f\ min}} < \gamma_{\mathrm{f}} < \gamma_{\mathrm{f\ max}}, \end{aligned} \tag{13}$$

where $h_{\mathrm{f}}, v_{\mathrm{f}}, \gamma_{\mathrm{f}}$ are the final height, final velocity, and final path angle, respectively; $h_{\mathrm{f\ max}}, v_{\mathrm{f\ max}}, \gamma_{\mathrm{f\ max}}$ are the maximum final height, maximum final velocity, and maximum final path angle, respectively; $h_{\mathrm{f\ min}}, v_{\mathrm{f\ min}}, \gamma_{\mathrm{f\ min}}$ are the minimum final height, maximum final velocity, and maximum final path angle, respectively. The final state constraints are decided by the mission parameter.

4. Onboard Trajectory Generation via AMPI

4.1. AMPI Strategy. The adaptive multivariate pseudospectral interpolation (AMPI) method was proposed by Sagliano

Table 2: The final errors of AMPI trajectories.

Number	Initial error of height, velocity and path angle	Final error of height, velocity, and path angle
1	(500.0 m, 30.0 m/s, 0.5 deg)	(100.3 m, 5.1 m/s, 0.0 deg)
2	(500.0 m, 30.0 m/s, -0.5 deg)	(97.4 m, 6.2 m/s, 0.0 deg)
3	(500.0 m, -30.0 m/s, 0.5 deg)	(121.6 m, 6.2 m/s, 0.0 deg)
4	(500.0 m, -30.0 m/s, -0.5 deg)	(106.0 m, 6.3 m/s, 0.0 deg)
5	(-500.0 m, 30.0 m/s, 0.5 deg)	(101.9 m, 6.6 m/s, 0.0 deg)
6	(-500.0 m, 30.0 m/s, -0.5 deg)	(114.8 m, 6.8 m/s, 0.1 deg)
7	(-500.0 m, -30.0 m/s, 0.5 deg)	(127 m, 7.5 m/s, 0.0 deg)
8	(-500.0 m, -30.0 m/s, -0.5 deg)	(111.8 m, 6.2 m/s, 0.1 deg)

et al. in 2016 [22]. The method consists of two parts, namely offline database generation and online trajectory generation. The scheme of AMPI is illustrated in Figure 1.

The offline database generation includes two operations. The first operation is the discretization of the parameter, and the second operation is the generation of trajectory database. And the conversion matrix, which is used to converse the low-density trajectory to high-density trajectory onboard, is also computed offline. The online trajectory generation includes three operations, namely reference space definition, low-density multivariate interpolation, and high multivariate interpolation.

The AMPI will not meet the numerical stability problem because there is no need to solve NLP or OCP. The calculation of AMPI is just polynomial calculation and matrix multiplication.

4.2. Parameter Space Definition. We defined a 3-dimension parameter space composed of height, velocity, and path angle which are the most important states affecting the trajectory. Then, we discretized the parameter space by 3 vectors, which contain a set of parameters in each dimension. The robustness of the algorithm could be guaranteed by the parameter space. Once the initial errors are within the parameter space, the AMPI will not diverge.

In this paper, three values are considered in each dimension for the initial state. The parameter space was discretized as follows:

$$\boldsymbol{X}_0 = \boldsymbol{X}_0^{*} + \begin{bmatrix} \delta h_i \\ \delta v_j \\ \delta \gamma_k \end{bmatrix} \quad i, j, k = [1, 2, 3], \tag{14}$$

where $\boldsymbol{X}_0^{*}$ is the nominal initial state and $\delta h_i, \delta v_j, \delta \gamma_k$ are the errors of the height, the velocity, and the path angle at initial time, respectively.

5. Simulation

5.1. Trajectory Optimization. The values of the initial states and the target terminal states are described in Table 1. The values of $h_{\mathrm{f\ max}}, v_{\mathrm{f\ max}}, \gamma_{\mathrm{f\ max}}$ are [26100m, 1800m/s, 0.5 deg], respectively, and the values of $h_{\mathrm{f\ min}}, v_{\mathrm{f\ min}}, \gamma_{\mathrm{f\ min}}$ are [25900m, 1790m/s, -0.5 deg], respectively. The value of $\alpha_{\max}$, $\lambda_{\max}, q_{\max}$ are [6 deg, 1, 120kPa], respectively, and $\alpha_{\min}, \lambda_{\min}, q_{\min}$ are [-2 deg, 0, 40kPa], respectively. The value of $\dot{\alpha}_{\max}$, $\dot{\lambda}_{\max}$ are [1 deg/s, 0.2], respectively.

Figure 2 shows the optimization trajectory of the nominal initial state. After about 90 seconds of ascending, the final height, final velocity, and final path angle are all satisfied with the terminal constraints. The final mass of the vehicle is 2800 kg, which means about 200 kg of fuel was consumed during the ascent phase.

The path angle decreases in the first 20 seconds, which makes the height become lower yet the velocity increases rapidly. As a consequence, the dynamic pressure becomes higher, allowing the engine to work at a better condition, which can be explained by the engine model. As height decreases, both density and velocity increase, causing the decrease of mass rate. Then, the path angle increases quickly and the craft ascends to higher height. At about 50 seconds, the path angle decreases again to meet the final height and final path angle constraints. Therefore, the mass rate becomes lower after the path angle decreases.

Figure 3 shows the time history of AOA and wingspan. The AOA increases rapidly while the path angle decreases due to the lack of lift. When the AOA comes to about 3-4 deg, the path angle and the height turn to increase. The AOA finally comes to 6 deg, which is the AOA value with maximum lift-drag ratio. The wingspan increases from the initial value 0.6 to 1, which is the upper bound of the wingspan, providing more lift to ascending of craft while the drag becomes larger at the same time. The wingspan decreases from the upper bound in order to decrease the lift and drag, as a consequence, the path angle decreases again.

Figure 4 shows the attack angle rate and wingspan rate. Both the attack angle rate and wingspan rate are satisfied with the constraints of control variables.

Figure 5 shows the time history of path constraints. In Figure 5(a), the dynamic pressure increases initially to almost the upper bound and, then, decreases quickly with the increase of height. In this way, the dynamic pressure is always within the dynamic pressure corridor controlled by the propulsion system. Figure 5(b) shows the vertical load, and Figure 5(c) shows the path angle rate. The vertical load and the path angle rate show a similar variation trend with the dynamic pressure, both of which are determined by the lift.

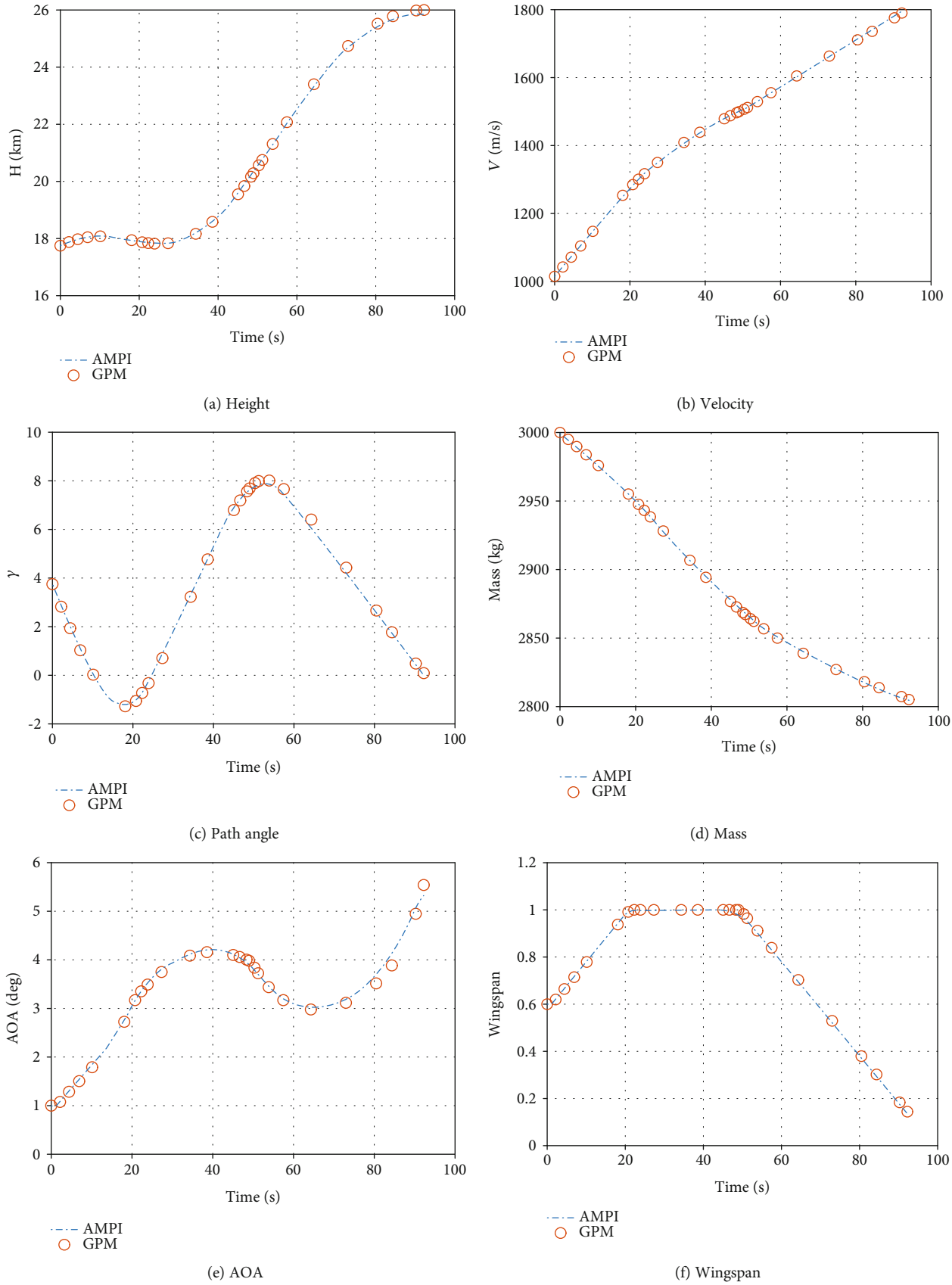

(a) Height

(b) Velocity

(c) Path angle

(d) Mass

(e) AOA

(f) Wingspan

Figure 8: AMPI vs. GPM.

5.2. Onboard Trajectory Generation. We considered 3 values in each dimension of the parameter space,

$$\begin{aligned} \delta \boldsymbol{h} &= [-500, 0, 500]\text{m} \\ \delta \boldsymbol{v} &= [-50, 0, 50]\text{m/s} \\ \delta \boldsymbol{\gamma} &= [-0.5, 0, 0.5]\ \text{deg}. \end{aligned} \tag{15}$$

These 3 vectors cover the initial states we need.

Firstly, we generated the AMPI trajectory database via the optimization strategy which contains all the situations defined by the parameter space. Figure 6 shows the offline AMPI trajectory database, including a database of both states and controls.

In Figure 6, we can see all the states of the offline database meet the terminal constraints at the final time and satisfy the path constraints all the time. The AOA increases initially to about 4 deg and then decreases gradually and, finally, increases again at the last few seconds. In contrast, the wingspan increases to the upper bound and maintains at the upper bound for few seconds and, then, decreases to almost the lower bound. All of the trajectories of the offline database are consistent with the optimization trajectory in Figure 2.

We considered the initial error as follows:

$$\begin{aligned} \delta h &= -250\text{m} \\ \delta v &= -25\text{m/s} \\ \delta \gamma &= 0.25\ \text{deg} \end{aligned} \tag{16}$$

Figure 7 shows the result of the initial state with the initial error defined by equation (16). The AMPI trajectory is almost the same with the integral trajectory, indicating excellent accuracy of the AMPI method. All of the time history of the states calculated by AMPI and the integral states coincide.

To fully illustrate the accuracy of the AMPI method, experiments were conducted under different conditions with different initial errors, as shown in Table 2. The values of the final errors are all within acceptable range, while the initial errors are distributed in different grids of the parameter space defined by equation (15), showing excellent adaption of the AMPI method to different initial conditions.

The mean value of the CPU time of the AMPI method required to compute the trajectory is about 0.1 second, which can meet the online trajectory generation requirement. The number of steps of calculation for the trajectory generation is decided by the number of low-density nodes and high-density nodes. Because the numbers of nodes of different initial errors are the same, and the CPU time of each simulation is almost the same. The more number of the nodes you choose, the higher accuracy you get, costing longer CPU time.

To prove the validity of the AMPI method, Figure 8 shows the AMPI trajectory and GPM trajectory with the initial error defined by equation (16). The time history of the controls and states calculated by AMPI and GPM are almost the same, and the final mass are, respectively, 2804.8 kg and 2805.1 kg. This means that the AMPI trajectory is almost the optimal trajectory.

6. Conclusions

This paper is utilizing the AMPI method to generate online trajectory of morphing aircraft without solving OCP or NLP. The simulation results indicate the high accuracy of the method, and the CPU time of the method shows real-time capability. The comparison between AMPI trajectory and GPM trajectory proves the validity of the AMPI method.

Data Availability

The image data used to support the findings of this study are available from the corresponding author upon request.

Conflicts of Interest

The authors declare that they have no conflicts of interests regarding the publication of this paper.

Authors' Contributions

Changzhu Wei is an Associate Professor of Harbin Institute of Technology; his research direction is automation control and trajectory optimization for aircrafts. Chenxin Zhang is a doctor of the National University of Defense Technology; his research direction is automation control and dynamics modeling for aircrafts. Yankun Zhang is a student of Harbin Institute of Technology; his research direction is trajectory optimization and guidance.

Acknowledgments

This research was funded by the National Nature Science Fund of China (Grant No. 61403100) and the Open National Defense Key Disciplines Laboratory of Exploration of Deep Space Landing and Return Control Technology, Harbin Institute of Technology (Grant No. HIT.KLOF.2013.079).

References

[1] S. Barbarino, O. Bilgen, R. M. Ajaj, M. I. Friswell, and D. J. Inman, "A review of morphing aircraft," *Journal of Intelligent Material Systems and Structures*, vol. 22, no. 9, pp. 823–877, 2011.

[2] S. Chiu, S. Chand, D. Moore, and A. Chaudhary, "Fuzzy logic for control of roll and moment for a flexible wing aircraft," *IEEE Control Systems*, vol. 11, no. 4, pp. 42–48, 1991.

[3] E. W. Pendleton, D. Bessette, P. B. Field, G. D. Miller, and K. E. Griffin, "Active aeroelastic wing flight research program: technical program and model analytical development," *Journal of Aircraft*, vol. 37, no. 4, pp. 554–561, 2000.

[4] J. N. Kudva, C. A. Martin, L. B. Scherer, A. P. Jardine, A. M. R. Mcgowan, R. C. Lake et al., *Overview of the DARPA/AFRL/-NASA Smart Wing program. Smart Structures and Materials 1999: Industrial and Commercial Applications of Smart Structures Technologies*, International Society for Optics and Photonics, 1999.

[5] M. A. Yi, P. Zhixiong, and L. Lie, *X-47b Flying Wing Aerodynamic Configuration Analysis*, Aeronautical Science & Technology, 2014.

[6] J. Bowman, B. Sanders, B. Cannon, J. Kudva, and T. Weisshaar, "Development of next generation morphing aircraft structures," in *48th AIAA/ASME/ASCE/AHS/ASC Structures, Structural Dynamics, and Materials Conference*, Honolulu, Hawaii, April 2007.

[7] K. Maute and G. W. Reich, "Integrated multidisciplinary topology optimization approach to adaptive wing design," *Journal of Aircraft*, vol. 43, no. 1, pp. 253–263, 2006.

[8] J. P. Jasa, J. T. Hwang, and J. Martins, "Design and trajectory optimization of a morphing wing aircraft," in *2018 AIAA/ASCE/AHS/ASC Structures, Structural Dynamics, and Materials Conference*, Kissimmee, Florida, January 2018.

[9] J. R. Maxwell and A. Phoenix, *Morphable Hypersonic Waverider and Trajectory Optimized for Atmospheric Entry*.

[10] M. Wu, T. Xiao, H. Ang, and H. Li, "Optimal flight planning for a Z-shaped morphing-wing solar-powered unmanned aerial vehicle," *Journal of Guidance, Control, and Dynamics*, vol. 41, no. 2, pp. 497–505, 2018.

[11] W. Peng, Z. Feng, T. Yang et al., *Trajectory Multiobjective Optimization of Hypersonic Morphing Aircraft Based on Variable Sweep Wing*, pp. 65–69, 2018.

[12] Huntington, *Advancement and Analysis of Gauss Pseudospectral Transcription for Optimal Control Problems*, Massachusetts Institute of Technology, 2007.

[13] C. L. Darby, W. W. Hager, and A. V. Rao, "An hp-adaptive pseudospectral method for solving optimal control problems," *Optimal Control Applications and Methods*, vol. 32, no. 4, pp. 476–502, 2011.

[14] I. M. Ross and M. Karpenko, "A review of pseudospectral optimal control: from theory to flight," *Annual Reviews in Control*, vol. 36, no. 2, pp. 182–197, 2012.

[15] X. Liu, P. Lu, and B. Pan, "Survey of convex optimization for aerospace applications," *Astrodynamics*, vol. 1, no. 1, pp. 23–40, 2017.

[16] B. Acikmese and S. R. Ploen, "Convex programming approach to powered descent guidance for Mars Landing," *Journal of Guidance, Control, and Dynamics*, vol. 30, no. 5, pp. 1353–1366, 2007.

[17] L. Blackmore, B. Açikmeşe, and D. P. Scharf, "Minimum-landing-error powered-descent guidance for Mars landing using convex optimization," *Journal of Guidance, Control, and Dynamics*, vol. 33, no. 4, pp. 1161–1171, 2010.

[18] X. Liu, *Autonomous Trajectory Planning by Convex Optimization*, Iowa State University, 2013.

[19] J. Wang, N. Cui, and C. Wei, "Rapid trajectory optimization for hypersonic entry using a pseudospectral-convex algorithm," *Proceedings of the Institution of Mechanical Engineers, Part G: Journal of Aerospace Engineering*, vol. 233, no. 14, pp. 5227–5238, 2019.

[20] R. Chai, A. Tsourdos, A. Savvaris, Y. Xia, and S. Chai, "Trajectory planning for hypersonic reentry vehicle satisfying deterministic and probabilistic constraints," *Acta Astronautica*, vol. 177, pp. 30–38, 2020.

[21] R. Chai, A. Tsourdos, A. Savvaris, S. Wang, Y. Xia, and S. Chai, "Fast Generation of Chance-Constrained Flight Trajectory for Unmanned Vehicles," *IEEE Transactions on Aerospace and Electronic Systems*, p. 1, 2020.

[22] M. Sagliano, E. Mooij, and S. Theil, "Onboard trajectory generation for entry vehicles via adaptive multivariate pseudospectral interpolation," *Journal of Guidance, Control, and Dynamics*, vol. 40, no. 2, pp. 466–476, 2017.